X-ray Properties of the Luminous Quasar PG 1634+706 at z=1.337 from SRG and XMM-Newton Data

G.S. Uskov, * ¹ S. Yu. Sazonov, ¹ M. R. Gilfanov, ^{1,2} I. Yu. Lapshov, ¹ R. A. Sunvaev, ^{1,2}

¹Space Research Institute, Russian Academy of Sciences, Moscow, 117997 Russia
²Max Planck Institut for Astrophysik, Karl-Schwarzschild-Str. 1, 85741 Garching, Germany

Abstract — In the fall of 2019, during the in-flight calibration phase of the SRG observatory, the onboard eROSITA and Mikhail Pavlinsky ART-XC telescopes carried out a series of observations of PG 1634+706 — one of the most luminous (an X-ray luminosity $\sim 10^{46}$ erg/s) quasars in the Universe at z < 2. Approximately at the same dates this quasar was also observed by the XMM-Newton observatory. Although the object had already been repeatedly studied in X-rays previously, its new observations allowed its energy spectrum to be measured more accurately in the wide range 1–30 keV (in the quasar rest frame). Its spectrum can be described by a two-component model that consists of a power-law continuum with a slope $\Gamma \approx 1.9$ and a broadened iron emission line at an energy of about 6.4 keV. The X-ray variability of the quasar was also investigated. On time scales of the order of several hours (here and below, in the source rest frame) the X-ray luminosity does not exhibit a statistically significant variability. However, it changed noticeably from observation to observation in the fall of 2019, having increased approximately by a factor of 1.5 in 25 days. A comparison of the new SRG and XMM-Newton measurements with the previous measurements of other X-ray observatories has shown that in the entire 17-year history of observations of the quasar PG 1634+706 its X-ray luminosity has varied by no more than a factor of 2.5, while the variations on time scales of several weeks and several years are comparable in amplitude.

Keywords: active galactic nuclei, supermassive black holes, X-ray observations

1 INTRODUCTION

Active galactic nuclei (AGNs) manifest themselves in a wide wavelength range, from radio to gamma-rays. A significant fraction (~ 10%, see, e.g., Elvis et al. 1994; Sazonov et al. 2004; Vasudevan & Fabian 2007; Shang et al. 2011; Sazonov et al. 2012) of the bolometric luminosity of AGNs is accounted for by the X-ray emission. This emission is believed to originate in the hot corona of the accretion disk as a result of the Comptonization of thermal (mainly ultraviolet) radiation from the disk. In addition, features associated with the reflection of hard coronal radiation from the disk and the surrounding dusty torus are observed in the X-ray spectra of AGNs (for a recent review, see, e.g., Malizia et al. 2020). Thus, the X-rays from AGNs carry important information about the accretion of matter onto supermassive black holes (SMBHs).

Based on data from space observatories, the X-ray spectra of many Seyfert galaxies, i.e., AGNs with a comparatively low luminosity ($L_{\rm X} \lesssim 10^{44}$ erg/s in the 2–10 keV band) located in the nearby Universe ($z \lesssim 0.1$), have been studied in detail (see, e.g., de Rosa et al. 2012; Ricci et al. 2017). As a rule, such objects are characterized by comparatively low black hole masses ($M_{\rm BH} \lesssim 10^9~M_{\odot}$) and accretion rates (less than 10% of the critical one at which the Eddington luminosity is reached; see, e.g., Khorunzhev et al. 2012; Prokhorenko & Sazonov 2021; Ananna et al. 2022). Since the properties of the accretion disks and their coronas can depend strongly on

both black hole mass and accretion rate (Shakura & Sunyaev 1973), it is important to investigate the X-ray emission of not only Seyfert galaxies but also AGNs with more massive black holes and/or higher Eddington ratios. In particular, of considerable interest are narrow-line Seyfert 1 galaxies, which are characterized by higher (close to the critical one) accretion rates than those for ordinary Seyfert galaxies at comparatively low black hole masses. Such objects have been well studied, and one of their distinctive features is comparative softness of their X-ray spectra (see, e.g., Jin et al. 2012).

Of special interest are high-luminosity ($L_{\rm X} \gtrsim 10^{46}\,{\rm erg/s}$) quasars in which a regime of accretion onto a black hole with a mass $M_{\rm BH} \gtrsim 10^9\,M_{\odot}$ close to the Eddington limit is probably realized. Such objects are very rare in the Universe, and even the nearest of them are at enormous distances from us, which makes their X-ray spectroscopy very difficult. Therefore, one of the most interesting quasars is PG 1634+706. This quasar is characterized by huge X-ray ($L_{\rm X} \sim 10^{46}\,{\rm erg/s}$) and bolometric ($\sim 10^{48}\,{\rm erg/s}$) luminosities (see, e.g., Shemmer et al. 2014¹), but, at the same time, it is located at a moderate redshift, z=1.337 (Neeleman et al. 2016, see Fig. 1). The black hole mass is estimated to be $\sim 10^{10}\,M_{\odot}$ (a rough estimate based on the H β width and

 $^{^1}$ In the cited paper a luminosity estimate at a wavelength of 2500Å, $\nu L_{\nu,2500} \sim 3 \times 10^{47}$ erg/s, is given, while the corresponding bolometric correction for quasars is estimated to be ~ 3 (Krawczyk et al. 2013).

2 Uskov et. al.

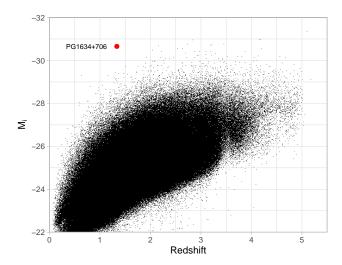


Figure 1: Position of the quasar PG 1634+706 (red dot) on the redshift i[z=2] absolute magnitude diagram. The black dots indicate the objects from the 16th data release of the SDSS quasar catalog (DR16v4, Lyke et al. 2020). The absolute magnitude of the quasar PG 1634+706, $M_i=-30.65$, was estimated using Eq. (4) from Richards et al. 2006 based on the luminosity measurement at a wavelength of 2500Ågiven in Table 2 from Shemmer et al. 2014. It should be noted that the quasar PG 1634+706 does not enter into the DR16v4 catalog, since this sky region was not covered during the spectroscopic SDSS.

luminosity), while the accretion rate is close to the critical one (Kelly et al. 2008). The quasar was discovered by the ultraviolet excess during the famous Palomar–Green survey (Green et al. 1986), and its first studies in X-rays with the Einstein orbital observatory were carried out already in the early 1980s (Tananbaum et al. 1986). Since then it has repeatedly become a target of X-ray observations, which has allowed its spectral characteristics and variability to be investigated.

The Russian Spectrum-RG X-ray observatory (hereafter SRG, Sunyaev et al. 2021) was launched on July 13, 2019, from the Baikonur Cosmodrome. During the flight of the spacecraft to the Lagrange point L2 of the Sun-Earth system in July-December 2019 the onboard eROSITA (Predehl et al. 2021) and Mikhail Pavlinsky ART-XC (Pavlinsky et al. 2021) telescopes observed a number of astrophysical objects to verify the performance of the instruments and to calibrate them. The quasar PG 1634+706, which was observed several times in the fall of 2019, was also among the targets. Its XMM-Newton observations (Jansen et al. 2001) were also carried approximately at the same dates. The data obtained from the three telescopes allowed us to investigate the X-ray spec- trum of PG 1634+706 and to study its variability with high reliability and accuracy. The results of this investigation are presented in our paper.

We use a ΛCDM cosmological model with parameters $H_0=70$ km/s/Mpc and $\Omega_{\Lambda}=0.7.$

2 OBSERVATIONS AND DATA ANALYSIS

Table 1 presents information about the X-ray observations of the quasar PG 1634+706 in the fall of 2019 whose data were used in this paper. These include four SRG observations, in which PG 1634+706 was no farther than 13' from the eROSITA axis, and three XMM-Newton observations. The latter were approximately synchronized with the SRG observations: the difference in the epochs of observations is about 5 days for the October observation and less than one day for the two November observations. During the SRG observation on September 29 only the sixth (TM6) of the seven eROSITA modules was switched on, while in the three later observations already all seven telescope cameras (TM1–TM7) operated.

Since the SRG observations under consideration were carried out at the Calibration and Performance Verification (Cal-PV) phase, their target, the quasar PG 1634+706 was at different angular distances from the optical axis of the eROSITA and ART-XC telescopes (approximately aligned) in different observations. More specifically, the source was almost at the center of the field of view in the first observation, at 2–3 arcmin from the axis in the second and third ones, and approximately at 13 arcmin from the center in the last one. Given the significant drop in the effective area of the ART-XC telescope at large angular distances from the axis, we used the data from the latest eROSITA observation (November 26) only to investigate the variability of the X-ray flux and did not use the eROSITA and ART-XC data from this observation for our spectral analysis.

For all three XMM-Newton observations we used only the data from the EPIC-PN camera (hereafter EPN), the most sensitive instrument of the observatory. No data from the EPIC-MOS cameras were used, since the observations of PG 1634+706 in the fall of 2019 were carried out in the mode of a small window with an angular size of $258^{\prime\prime} \times 258^{\prime\prime}$ for EPN and $110^{\prime\prime} \times 110^{\prime\prime}$ for EPIC-MOS, which makes a reliable determination of the background (for our spectral analysis) in the latter case virtually impossible.

2.1 SRG/eROSITA

We calibrated and processed the eROSITA data using the eROSITA Science Analysis Software System (eSASS) software package of version esass_211201 and the software developed by us. The calibration database of version caldb_211201 was used.

The lists of events were filtered using the QUALGTI good time intervals with the evtool $(v2.29.2/2.18)^2$ code. We excluded the time intervals during which the SRG observatory was slewed. The pure vignetting-corrected exposure time for each observation is given in Table 1.

The srctool procedure was used to extract the X-ray spectra and light curves. The photons from the source were extracted from a region with a radius of 1^{\prime} (Fig. 2). The

² erosita.mpe.mpg.de/edr/DataAnalysis/evtool_doc

Period of observations	Observatory	Telescopes, instruments	Exposure time, ks
2019-09-29 21:38 - 09-30 13:05	SRG	ART-XC, eROSITA (TM6)	48.3, 55.0
$2019 \text{-} 10 \text{-} 20 \ 14 \text{:} 42 - 10 \text{-} 21 \ 01 \text{:} 52$	SRG	ART-XC, eROSITA (TM1-7)	37.7, 39.0
$2019 \text{-} 10 \text{-} 25 \ 18 : 02 - 10 \text{-} 26 \ 00 : 58$	XMM-Newton	EPIC-PN	14.4
$2019 \text{-} 11 \text{-} 23\ 09 \text{:} 11 - 20 \text{:} 18$	SRG	ART-XC, eROSITA (TM1-7)	37.0, 38.3
$2019 \text{-} 11 \text{-} 24 \ 14 \text{:} 38 - 19 \text{:} 54$	XMM-Newton	EPIC-PN	12.7
$2019 \text{-} 11 \text{-} 26\ 07 \text{:} 05 - 18 \text{:} 14$	SRG	eROSITA(TM1-7)	39.8
$2019 \text{-} 11 \text{-} 26 \ 14 \text{:} 32 - 22 \text{:} 19$	XMM-Newton	EPIC-PN	17.3

The first column gives the universal times of the start and end of the observation. The second and third columns give the name of the observatory and the corresponding telescopes and instrument; the switched-on cameras for eROSITA are given in parentheses. The last column gives the effective exposure time corrected for vignetting.

Table 1: Log of observations of PG 1634+706 in 2019

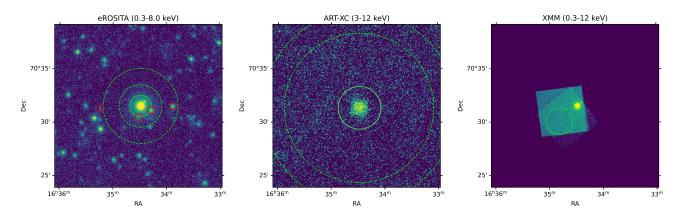


Figure 2: The X-ray images of the quasar PG 1634+706 obtained from the series of observations (see Table 1) with the eROSITA and ART-XC telescopes of the SRG observatory and the EPN telescope of the XMM-Newton observatory (in the 0.3–8, 3–12, and 0.3–12 keV energy bands, respectively). On each panel the green solid circumference marks the source spectrum extraction region, while the dashed circumferences mark the background extraction region (for XMM-Newton these regions slightly differ in different observations; the regions for the observation on October 25, 2019, OBSID=0852980501, are shown). The red circles in the eROSITA image indicate the regions around other detected sources the events in which were excluded from our spectral and timing analyses.

background was estimated in a ring around the source with inner and outer radii of 2' and 3.5' respectively. The events within 20" of other sources closest to the quasar detected by eROSITA (Fig. 2) were excluded from consideration.

The spectra of the source obtained were binned in such a way that there were at least 30 counts (as for ART-XC, see below) from the source and the background in each energy bin. The light curves were binned in 1 ks, except for the September 29, 2019 observation that was binned in 4 ks. With such binning there are at least 15 total counts from the source and the background in each time bin. At the end of each observation we removed the bins related to "bad" time (according to GTI). To calculate the 68% confidence intervals for the count rate, we used the Monte Carlo method whereby the counts from the source and the background are randomly selected according to the Poisson distribution.

2.2 SRG/ART-XC

The spectra were extracted with the standard ART-XC software package adapted to the goals of this study using the current version of the calibrations. In individual energy intervals we constructed the photon, exposure, and vignetting maps. To take into account the contribution of the particle background to the source spectrum, we constructed the model particle background maps obtained during the allsky survey in periods when no sources were observed in the field of view. The spectrum of the quasar PG 1634+706 was extracted in a circle of radius 2'. The background normalization was estimated in a ring with inner and outer radii of 7' and 9' respectively (Fig. 2). In the ring region the model background map was normalized to the background map with allowance made for the exposure time. The normalized background map was used in the region with the source to subtract the underlying background. The remaining photons were assumed to belong to the source and were

4 Uskov et. al.

corrected for the vignetting map for the reduction to the nominal effective area.

The angular resolution of ART-XC does not allow one to reliably separate the emissions from the quasar PG 1634+706 and other point sources that are detected by eROSITA within 2' of it (Fig. 2). However, according to the eROSITA data, the contribution of these sources to the flux from the quasar in the energy range from 0.3 to 8 keV does not exceed 5%. Consequently, the unresolved sources should not affect noticeably the spectrum measured by the ART-XC telescope. We restricted ourselves to using the energy channels above 5 keV when performing our spectral analysis. This is because the ART-XC response matrix is not well calibrated near the lower boundary of the sensitivity range of its detectors ($\sim 3-4 \text{ keV}$). The remaining energy channels were binned in such a way that there were at least 30 counts in each of the bins (this is dictated by the necessity of using the χ^2 test in modeling the SRG spectra, since the background has already been subtracted in the ART-XC spectral data data used by us).

2.3 XMM-Newton/EPN

The primary processing of the data from the EPN camera of the XMM-Newton observatory was performed using the Science Analysis System (SAS) v20.0 software. We used the latest calibration versions at the SAS v20.0 release time.

The file of events was filtered: only the single and double events (PATTERN ≤ 4) in the energy range 0.3–12 keV were left; the times with an enhanced background³ and the events in and near bad pixels (FLAG=0) were removed.

The spectral and timing data were extracted with the xmmselect code. The source and background regions were chosen so as to maximize the signal-to-noise ratio. The right panel in Fig. 2 shows the combined image from the three 2019 XMM-Newton observations.

The spectra of the source were binned in such a way that there were at least five counts in each energy bin. This is needed to fit the spectra using the W-statistic (below in the text called Cstat), which takes into account the presence of an X-ray background with a Poisson distribution. The light curves were binned in 1 ks. We also removed the time bins with a fractional exposure FRACEXP; 0.1. With such binning there are at least 15 net counts from the source in each time bin.

3 RAPID VARIABILITY

To investigate the X-ray variability of the quasar PG 1634+706 on time scales shorter than one day, we constructed the light curves from the SRG/eROSITA and XMM-Newton/EPN data for the individual observations.

Figure 3 shows the time dependences of the count rate in two energy bands, 0.3-2.3 and 2.3-6.0 keV.

To understand whether there is a statistically significant variability of the X-ray flux in a given observation and a given energy band, we calculated the χ^2 statistic:

$$\chi^2 = \sum_{i=1}^{N} \frac{(f_i - \overline{f})^2}{\sigma_i^2},$$
 (1)

where f_i is the count rate in the ith time bin, σ_i is the corresponding error, \overline{f} is the weighted mean count rate for the entire observation, and N is the number of measurements. The probability to obtain by chance a value of the χ^2 distribution greater than the measured one for dof = N-1 degrees of freedom characterizes the probability (1-p) that the count rate was constant in a given observation.

To estimate the X-ray variability amplitude, we calculated the variance normalized to the mean flux and corrected for the flux measurement errors (Vaughan et al. 2003):

$$\sigma_{\rm rms}^2 = \frac{S^2 - \overline{\sigma_{\rm err}^2}}{\langle f \rangle^2},\tag{2}$$

where

$$S^{2} = \frac{1}{N-1} \sum_{i=1}^{N} (f_{i} - \langle f \rangle)^{2},$$
 (3)

$$\overline{\sigma_{\rm err}^2} = \frac{1}{N} \sum_{\rm i}^N \sigma_{\rm i}^2 \tag{4}$$

and $\langle f \rangle$ is the arithmetic mean count rate.

The error in $\sigma_{\rm rms}^2$ can be estimated using the formula from Turner et al. (1999):

$$\delta\sigma_{\rm rms}^2 = \frac{s_D}{\langle f \rangle^2 \sqrt{N}},\tag{5}$$

where

$$s_D^2 = \frac{1}{N-1} \sum_{i=1}^{N} \{ [(f_i - \langle f \rangle)^2 - \sigma_i^2] - \sigma_{\text{rms}}^2 \langle f \rangle^2 \}^2.$$
 (6)

The derived values of χ^2 (dof), 1-p, and $\sigma^2_{\rm rms}$ are given in Table 2. No statistically significant variability (at a confidence level greater than 2σ) was detected in any of the SRG/eROSITA and XMM-Newton observations.

The light curves were also studied for the presence of a linear trend. Only for the XMM-Newton observation on November 26, 2019, in the 0.3–2.3 keV energy band did we find a statistically significant (p < 0.0001) improvement in the quality of the light-curve fit. More specifically, there is evidence for an increase in the count rate during the observation. At the same time, we did not find a similar positive trend in the SRG/eROSITAobservation that was carried out only several hours earlier and partially overlaps in time with the XMM-Newton observation.

 $^{^3}$ www.cosmos.esa.int/web/xmm-newton/sas-thread-epic-filterbackground

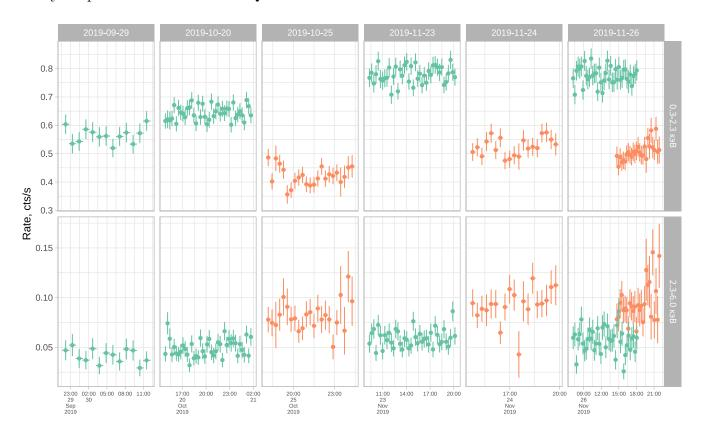


Figure 3: The SRG/eROSITA (green) and XMM-Newton/EPN (orange) light curves (in counts per second) for the individual observations in two energy bands: 0.3-2.3 (top) and 2.3-6.0 keV (bottom). It should be noted that the absolute values of the eROSITA and EPN count rates cannot be directly compared with each other.

Telescope	Date	$\chi^2 \text{ (dof)}$	1-p	$\sigma_{\rm rms}^2, 10^{-4}$	
Energy range 0.3–2.3 keV					
eROSITA	2019-09-29	8.3(12)	0.759	-11 ± 7	
	2019-10-20	33.9(39)	0.702	-2 ± 2	
	2019-11-23	38.7(39)	0.482	-0.2 ± 3	
	2019-11-26	31.9(39)	0.782	-4 ± 3	
EPN	2019-10-25	25.1(22)	0.291	6 ± 16	
	2019-11-24	17.4(18)	0.499	-3 ± 8	
	2019-11-26	18.1(26)	0.872	-11 ± 12	
	Energy ra	ange 2.3–6.0	0 keV		
eROSITA	2019-09-29	7.1(12)	0.853	-222 ± 81	
	2019-10-20	45.6(39)	0.217	63 ± 67	
	2019-11-23	39(39)	0.468	11 ± 55	
	2019-11-26	52.7(39)	0.070	60 ± 111	
EPN	2019-10-25	15(22)	0.862	-108 ± 104	
	2019-11-24	18.9(18)	0.399	60 ± 141	
	2019-11-26	22.9(26)	0.637	56 ± 118	

Table 2: Characteristics of the rapid X-ray variability

4 X-RAY SPECTRUM

The spectra were fitted using the XSPEC v12.12.0 software (Arnaud 1996). We analyzed the eROSITA and ART-XC data jointly and the XMM-Newton/EPN data separately. We used the χ^2 -statistic to fit the models to the data from the SRG telescopes and Cstat for the XMM-Newton/EPN data.

First we tried to fit the source spectrum by a power law with a low-energy cutoff due to photoabsorption in the Galaxy. In the terminology of XSPEC we used the following model:

TBabs(zpowerlaw),

where TBabs is the interstellar absorption model by Wilms et al. (2000). Following the example of the authors of previous papers on the X-ray observations of the quasar PG 1634+706 (in particular, Piconcelli et al. 2005), we fixed the hydrogen column density toward this object at its Galactic value of $N_{\rm H} = 5.74 \times 10^{20}~{\rm cm}^{-2}$ ((Elvis et al. 1989).

The results of fitting the the measured spectra by this empirical model are shown in Figs. 4 and 5. In our modeling we assumed that the slope of the spectrum remained constant in all SRG observations, but its normalization (i.e., the X-ray flux) could change. Since in reality the slope could slightly change from observation to observation and given that different observations were carried out at different angles to the optical axis of the telescopes, we added the crosscalibration coefficient between the eROSITA and ART-XC telescopes to the model as a free parameter. The same assumption (about the constancy of the spectral slope) was also made with regard to the XMM-Newton observations. Thus, we jointly fitted, first, three SRG spectra and, second, three XMM-Newton spectra. The derived model parameters are given in Table 3. Here and below, we specify the confidence intervals for the parameters at a 68% level and the upper limits at a 2σ level, unless stated otherwise.

Although the power law with absorption, on the whole, describes satisfactorily the shape of the measured spectra, a number of statistically significant additional features are observed: (1) a soft X-ray excess at energies $\sim 0.3\text{--}0.4$ keV, (2) an emission excess near 2.7 keV, and (3) a decrease in intensity near 0.5 keV. The first two features manifest themselves in both SRG and XMM-Newton (less clearly) spectra, while the last one manifests itself in the SRG spectrum taken on November 23, 2019, and at a low confidence level in the October 20, 2019 SRG spectrum.

The emission excess at energies below $\sim 1~\rm keV$ (in the source rest frame) observed in the spectrum of PG 1634+706 is not unique for this object. Such an additional emission component is detected in the spectra (of good quality) for most Type-1 AGNs, while its nature is actively discussed (see, e.g., Turner & Pounds 1989; Guainazzi & Bianchi 2007; Boissay et al. 2016). In particular, it can result from the Comptonization of ultraviolet radiation from the accretion

disk in the "warm corona" (with a temperature of the order of several million K), in contrast to the main (power-law) component of the hard X-ray emission that is believed to be formed in the "hot corona" ($T \sim 10^9$ K) of the accretion disk

The energy of 2.7 keV, at which an emission excess is also observed in the spectrum of the quasar PG 1634+706, roughly corresponds to the position of the $K\alpha$ line of neutral or weakly ionized iron (6.4 keV) at the redshift of the object: 6.4/(1+z)=2.74 keV. This suggests that we are dealing with an iron emission line or a set of such lines. As regards the "absorption" feature near 0.5 keV in the eROSITA spectra, it, along with the emission excess at low energies, can be a manifestation of a more complex spectral shape than the simple continuum models that we we tried to apply.

The insufficiently high statistical significance of the detection of the soft emission component in the spectrum of the quasar PG 1634+706 does not allow it to be studied in more detail. Therefore, we excluded the range of energies below 0.7 keV from our subsequent consideration by concentrating on the study of the spectral continuum shape in the energy range from 0.7 to $\sim 13~{\rm keV}$ and the emission feature near the Fe K α line.

The subsequent analysis was performed separately for each SRG and XMM-Newton spectrum, i.e., we assumed that not only the normalization but also the spectral shape could change from observation to observation. The cross-calibration constant between the eROSITA and ART-XC data was no longer used.

We used three models. First, we again applied the power-law model with Galactic absorption (TBabs(zpowerlaw)) in the terminology of XSPEC) below called the PL model. Then, to describe the emission feature near 6.4 keV (in the quasar rest frame), we added a line with a Gaussian profile to this model: TBabs(zpowerlaw + zgauss) (hereafter PL+GAUSS).

If the observed iron emission line is associated with the reflection of hard X-ray coronal radiation from the accretion disk or the dusty torus, then it is natural to also expect an additional emission in spectral continuum (at energies above $\sim 10 \text{ keV}$ in the quasar rest frame). Therefore, we considered one more model, where the component associated with the reflection of a power-law continuum from a cold disk (Magdziarz & Zdziarski 1995) was added to the two previous components, i.e., we used the TBabs(zpowerlaw +zgauss + pexrav) or PL+GAUSS+PEXRAV model. The relative normalization of the reflected PEXRAV component with respect to the power-law PL component was described by the parameter rel_{ref} that for this purpose was specified to be negative (see the description of PEXRAV in XSPEC); below we will use the notation $R_{\text{refl}} \equiv -rel_{\text{refl}}$. The spectral slope of the incident radiation in the PEXRAV component was tied to the slope of the PL component. The abundance of heavy elements was fixed at the solar one, according to Anders & Grevesse (1989). The cosine of the inclination angle was fixed at 0.5. The high-energy cutoff was not considered. Because of the low detection significance of the iron emission

⁴ https://heasarc.gsfc.nasa.gov/xanadu/xspec

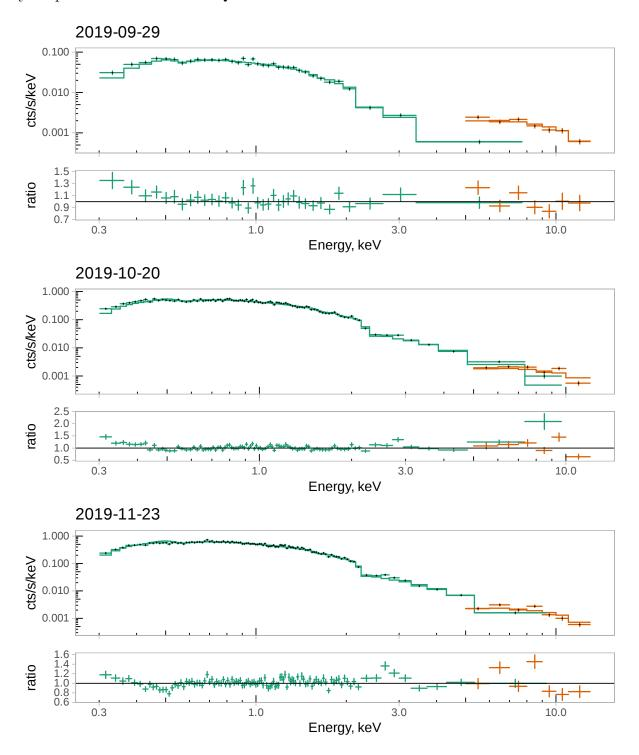


Figure 4: The X-ray spectrum of the quasar PG 1634+706 measured with the eROSITA (green color) and ART-XC (orange color) telescopes of the SRG observatory at different dates. All three spectra were fitted jointly by a power law with Galactic absorption with a single slope but different normalizations (see Table 3). For better clarity, the spectra in the figure were rebinned. The data-to-model ratio is shown under each spectrum.

line in the XMM-Newton spectra, when fitting these spectra by the PL+GAUSS and PL+GAUSS+PEXRAV models, the central energy and width of the line were fixed at the weighted mean values obtained when fitting the SRG spectra by the PL+GAUSS+PEXRAV model.

Figures 6 and 7 show how the SRG and XMM-Newton spectra are fitted by the three-component PL+GAUSS+PEXRAV model. Tables 4 and 5 present the parameters of the fits to the spectra by the PL, PL+GAUSS and PL+GAUSS+PEXRAV.

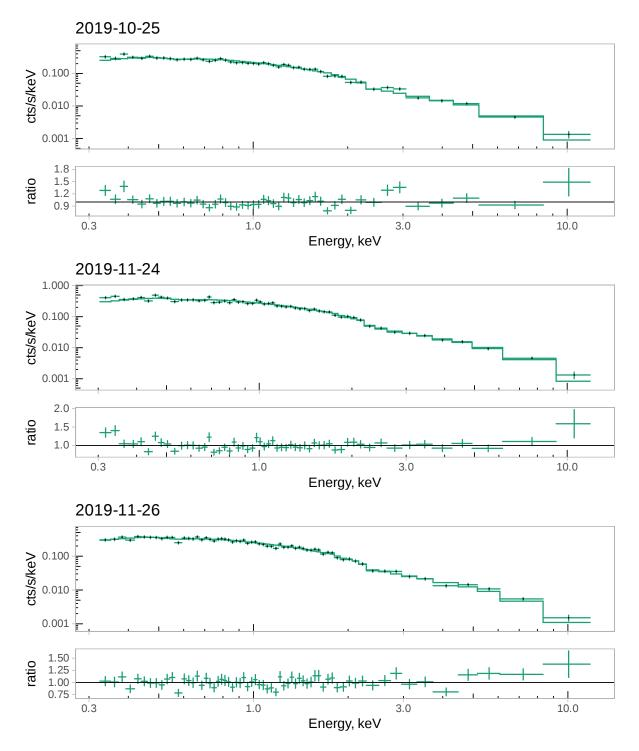


Figure 5: Same as Fig. 4 but for the XMM-Newton data.

Adding the iron emission line to the power-law model leads to a statistically significant improvement in the quality of the fit to the SRG spectra taken on October 20 and November 23, 2019 (recall that the spectrum constructed from the September 29 observation is characterized by considerably poorer statistics, because only one of the eROSITA modules operated in this observation) and the XMM-Newton spectrum measured on October 25, 2019.

The line width from the SRG/eROSITA data turns out to be nonzero, while the position of the line center is limited in the range from ~ 6.3 to ~ 6.6 keV for the October 20 and November 23, 2019 spectra, i.e., it is compatible with an energy of 6.4 keV.

The reflected continuum component (PEXRAV) is not detected at a statistically significant level in any of the spectra obtained, except for the latest XMM-Newton observation

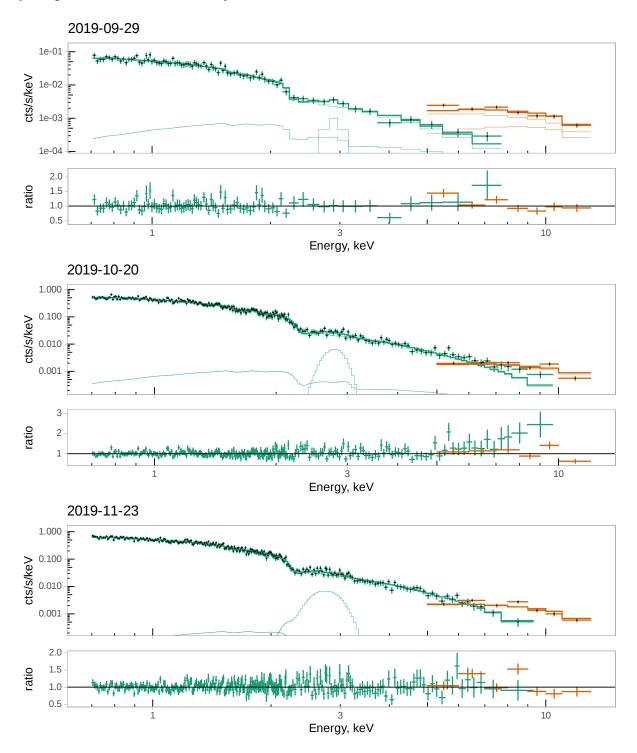


Figure 6: The fits to the spectra of the quasar PG 1634+706 measured with the eROSITA (green color) and ART-XC (orange color) telescopes of the SRG observatory at different dates by the PL+GAUSS+PEXRAV model with Galactic absorption (see Table 4). The solid lines, except for the combined model, indicate its individual components: the power-law continuum (PL), the Gaussian line (GAUSS), and the reflected component (PEXRAV) (if present). The spectra were rebinned for clarity. The data-to-model ratio is shown under each spectrum.

SRG/eROSITA, ART-XC				
Date	2019-09-29	2019-10-20	2019-11-23	
Energy range, keV	0.3 – 13	0.3 – 12	0.3 – 13	
Counts	4409.0 + 556.0	25108.8 + 395.0	29712.6 + 507.0	
Γ		1.843 ± 0.008		
F_X , $10^{-13} \text{ erg/s/cm}^2$	$5.17^{+0.11}_{-0.11}$	$5.92^{+0.09}_{-0.09}$	$7.03^{+0.11}_{-0.11}$	
Constant	1.21 ± 0.06	0.96 ± 0.05	1.02 ± 0.05	
$\chi^2 \text{ (dof)}$	1032 (790)			
XMM-Newton/EPN				
Date	2019-10-25	2019-11-24	2019-11-26	
Energy range, keV	0.3 – 11.8	0.3 – 11.8	0.3 – 11.8	
Counts	5872.8	6602.6	8269.2	
Γ		1.828 ± 0.011		
$F (4-12 \text{ keV}), 10^{-13} \text{ erg/s/cm}^2$	$6.42^{+0.16}_{-0.16}$	$8.01^{+0.20}_{-0.19}$	$7.72^{+0.19}_{-0.19}$	
Cstat (dof)	-0.10	$2101 \ (2133)$	-0.19	

Counts is the number of counts from the source minus the background (the sums of the eROSITA and ART-XC counts are given for the SRG observations), Γ is the spectral slope, F is the flux in the observed 4–12 keV energy band corrected for Galactic absorption, Constant is the correction factor for the ART-XC data relative to eROSITA, and dof is the number of degrees of freedom.

Table 3: Results of fitting the measured SRG and XMM-Newton spectra by a power law with absorption

(on November 26, 2019), where there is weak evidence (at a level of ~ 2 standard deviations) for its presence.

Figure 8 shows how the parameters of the PL+GAUSS+PEXRAV model changed from observation to observation. The slope of the spectrum (power-law component) and the equivalent width of the iron line do not show any statistically significant evolution, remaining at ~ 1.9 and ~ 120 eV, respectively. At the same time, there is a statistically significant flux increase in the power-law spectral component.

5 LONG-TERM EVOLUTION

As has already been noted in the Introduction, the quasar PG 1634+706 has been repeatedly observed by different X-ray observatories since 1981. This allows the evolution of its activity in X-rays to be traced over approximately 17 years in the source rest frame. Brief information about all X-ray observations of PG 1634+706 namely the Einstein, ROSAT, ASCA, Chandra, XMM-Newton, Swift, and SRG observations, is collected in Table 6.

Shemmer et al. (2014) estimated the X-ray fluxes in the observed 0.2–10 keV energy band corrected for Galactic absorption for all observations until 2012 inclusive. The quasar spectrum was assumed to be fitted by a power law with a photon index of $\Gamma=2$. Only the SRG and XMM-Newton observations carried out in the fall of 2019 are the new ones compared to the paper by Shemmer et al. (2014). We used the X-ray fluxes from Shemmer et al. (2014) to estimate the quasar luminosity in the 2–10 keV energy band (in the source rest frame) for all archival observations. Us-

ing the same spectral model (a power law with $\Gamma=2$ and Galactic absorption) and the data being discussed in this paper, we calculated the luminosities for the SRG and XMM-Newton observations in 2019. Our luminosity estimates and their statistical errors are given in Table 6. Note that these errors turned out to be considerably smaller ($\lesssim 2\%$) than the corresponding errors in the flux of the power-law component obtained by us previously when modeling the SRG and XMM-Newton spectra (cf. the results in Tables 4 and 5). This is because in that case the spectral slope was a free parameter and a number of free parameters were also used simultaneously.

It should be noted that since different measurements were obtained from the data of different instruments and in originally different energy bands, this must lead to an additional systematic error in the luminosity estimate. This uncertainty probably does not exceed 10–20% (Shemmer et al. 2014) for the data obtained after 2000, given the careful cross-calibration of the modern X-ray observatories and that all these data were obtained in approximately identical energy bands. However, the systematic error can be more significant for earlier observations, in particular, the Einstein and ROSAT ones, especially when the soft X-ray band (0.3–3.3 and 0.5–2.0 keV, respectively) in which these measurements were carried out is taken into account.

Figure 9 shows how the luminosity of the quasar PG 1634+706 evolved in 1981–2019. Although the light curve is characterized by a large sampling interval, it can be said with confidence that the X-ray emission is variable on time scales from several days to several years (in the source rest frame). The ratio of the maximum ($\sim 1.25 \times 10^{46}$ erg/s

Date	2019-09-29	2019-10-20	2019-11-23		
Energy range, keV	$0.713~\mathrm{keV}$	$0.712~\mathrm{keV}$	$0.713~\mathrm{keV}$		
PL model					
Γ	1.78 ± 0.02	1.864 ± 0.015	$1.850^{+0.014}_{-0.013}$		
$F_{\rm PL}~(412~{\rm keV}),~10^{-13}~{\rm erg/s/cm^2}$	5.7 ± 0.2	5.74 ± 0.15	7.05 ± 0.16		
$\chi^2 \text{ (dof)}$	98.8 (91)	$316.2\ (263)$	326 (272)		
PL+	-GAUSS model				
Γ	1.78 ± 0.02	1.876 ± 0.016	1.866 ± 0.014		
$F_{\rm PL}~(412~{\rm keV}),~10^{-13}~{\rm erg/s/cm^2}$	5.7 ± 0.2	5.60 ± 0.16	6.82 ± 0.17		
$E_{ m line},{ m keV}$	$6.8^{+0.2}_{-0.4}$	$6.52^{+0.11}_{-0.13}$	6.44 ± 0.16		
$\sigma_{ m line},{ m keV}$	< 0.6~(68%)	$0.30^{+0.20}_{-0.12}$	$0.52^{+0.12}_{-0.13}$		
EW, keV	0.08 ± 0.07	$0.11^{+0.03}_{-0.04}$	0.14 ± 0.04		
$\chi^2 \text{ (dof)}$	97 (88)	$302.1\ (260)$	$306.7\ (269)$		
PL+GAUSS+PEXRAV model					
Γ	$1.95^{+0.09}_{-0.08}$	1.90 ± 0.03	$1.870^{+0.025}_{-0.018}$		
$F_{\rm PL}~(412~{\rm keV}),~10^{-13}~{\rm erg/s/cm^2}$	$4.1^{+0.6}_{-0.7}$	5.4 ± 0.3	$6.8^{+0.2}_{-0.3}$		
$E_{ m line},{ m keV}$	6.8 ± 0.3	$6.51^{+0.12}_{-0.14}$	$6.44_{-0.16}^{+0.15}$		
$\sigma_{ m line},{ m keV}$	< 0.8~(68%)	$0.32^{+0.23}_{-0.13}$	$0.51^{+0.14}_{-0.11}$		
EW, keV	0.12 ± 0.08	0.12 ± 0.04	$0.14^{+0.04}_{-0.06}$		
$R_{ m refl}$	$0.19^{+0.08}_{-0.11}$	< 0.12	< 0.07		
$\chi^2 \text{ (dof)}$	89.7 (87)	301.1 (259)	306.7 (268)		

 Γ and $F_{\rm PL}$ are the slope of the power-law component and the Galactic extinction-corrected flux in the observed 4–12 keV energy band in this component; $E_{\rm line}$, $\sigma_{\rm line}$ and EW are the central energy, width, and equivalent width of the Gaussian line; $R_{\rm refl}$ is the reflection coefficient; dof is the number of degrees of freedom.

Table 4: Results of fitting the measured SRG spectra by different models

in November 2002) to minimum ($\sim 5 \times 10^{45}$ erg/s in January 2009) X-ray luminosity in the entire history of observations of the quasar is ~ 2.5 . At the same time, $\sigma_{\rm rms}^2 = 0.030 \pm 0.016$ (from Eq. 2), i.e., the rms characteristic amplitude of the luminosity variations was $\sim 16\%$. In the fall of 2019, during the SRG and XMM-Newton observations, the object was in an "average" state for itself, when its luminosity varied in the range from 6×10^{45} to 9×10^{45} erg/s and rose almost monotonically.

6 DISCUSSION AND CONCLUSIONS

Although the quasar PG 1634+706 has already been repeatedly studied in X-rays previously, its new SRG and XMM-Newton observations have allowed us to measure more accurately its energy spectrum in the wide range $\sim 1\text{--}30~\text{keV}$ (in the quasar rest frame). One of the most interesting results was the detection of a broad ($\sim 1~\text{keV}$ at half maximum) iron emission line in the spectrum with an equivalent width $\sim 120~\text{eV}$. The weighted mean position of the line centroid from different observations is consistent with the energy of

 $6.4~{\rm keV}$ corresponding to the K_{α} transition in the neutral iron atom (and is inconsistent with the energy of 6.7 keV of the helium-like iron triplet in the case of hot rarefied plasma radiation). The line broadening is statistically significant.

It is natural to assume that this emission feature is associated with the reflection of hard X-ray coronal radiation from the accretion disk and, possibly, the dusty torus. In this case, the reflected component must also emerge in the spectral continuum. The search for this component based on the SRG and XMM-Newton data did not lead to a significant detection. The reflection coefficient in the PEXRAV model is $R_{\rm refl} \lesssim 0.3$. This limit and the measured equivalent width of the iron emission line are consistent with the scenario for the reflection of coronal radiation from an optically thick, cold disk (see, e.g., George & Fabian 1991). In this case, the significant line broadening can be associated with the Doppler broadening in the accretion disk (this requires radial velocities $v_{\rm r}/c \sim 0.06$), as is often discussed in the context of X-ray binaries and AGNs (for a review, see, e.g., Miller 2007), and with the reflection from a strongly ionized gas in the inner disk (in this case, a set of $K\alpha$ lines

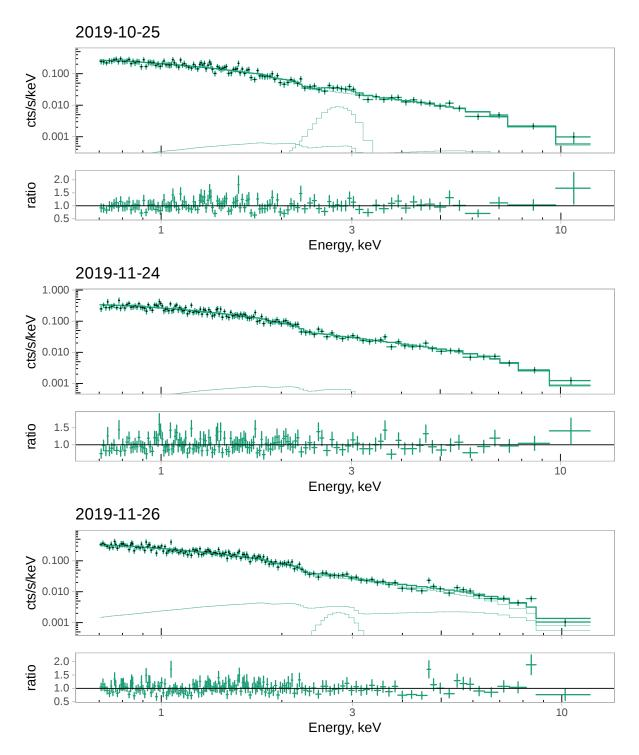


Figure 7: Same as Fig. 6 but for the XMM-Newton data.

of different iron ions arises; see, e.g., Nayakshin et al. 2000; Ross & Fabian 2005).

As regards the main (power-law) component of the spectrum, the values of its slope measured in different SRG and XMM-Newton observations agree with each other within the error limits and lie in the range from 1.8 to 2.0. Such values are typical for Seyfert galaxies and moderate-luminosity quasars. Thus, for the quasar PG 1634+706 we see no confirmation of the second sec

mation of the tendency for the X-ray continuum to steepen significantly with increasing luminosity and/or Eddington ratio that was pointed out for AGNs by a number of authors (Shemmer et al. 2008; Brightman et al. 2013) but was called into question in other papers (see, e.g., Trakhtenbrot et al. 2017).

Apart from the spectral properties, we investigated the X-ray variability of the quasar PG 1634+706. On time scales

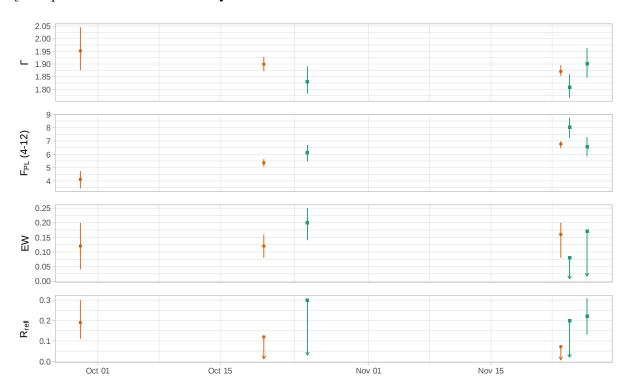


Figure 8: Variations in the parameters of the PL+GAUSS+PEXRAV spectral model during the SRG (orange color) and XMM-Newton (green color) observations in the fall of 2019. The slope of the power-law component, the flux in the power-law component (in units of 10^{-13} erg/s/cm²), the equivalent width of the iron line, and the relative normalization of the reflected component (see Tables 4 and 5) are shown (from top to bottom).

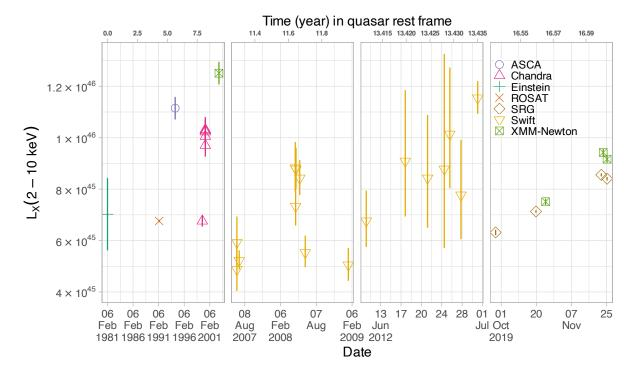


Figure 9: Long-term evolution of the X-ray luminosity of the quasar PG 1634+706 The luminosity is given in the 2–10 keV energy band in the source rest frame. The 1σ statistical measurement errors are shown. The date of observations is along the lower axis; the time since the first observation in the source rest frame is along the upper axis.

2019-10-25	2019-11-24	2019-11-26			
$0.711.8~\mathrm{keV}$	$0.711.8~\mathrm{keV}$	$0.711.8~\mathrm{keV}$			
PL model					
1.78 ± 0.03	1.79 ± 0.03	1.78 ± 0.03			
6.8 ± 0.3	8.4 ± 0.4	$8.3^{+0.4}_{-0.3}$			
562.5 (584)	547.7(574)	710.9 (747)			
-GAUSS model					
1.81 ± 0.03	1.79 ± 0.03	1.79 ± 0.03			
$6.4^{+0.4}_{-0.3}$	8.4 ± 0.4	8.2 ± 0.4			
6.5 (fixed)	6.5 (fixed)	6.5 (fixed)			
0.50 (fixed)	0.50 (fixed)	0.50 (fixed)			
0.20 ± 0.06	< 0.11	< 0.13			
551.7 (583)	547.7(573)	710.6 (746)			
PL+GAUSS+PEXRAV model					
$1.83^{+0.06}_{-0.05}$	$1.81^{+0.05}_{-0.04}$	1.90 ± 0.06			
$6.1^{+0.6}_{-0.7}$	$8.0^{+0.7}_{-0.8}$	6.6 ± 0.7			
6.50 (fixed)	6.50 (fixed)	6.50 (fixed)			
0.50 (fixed)	0.50 (fixed)	0.50 (fixed)			
$0.20^{+0.05}_{-0.06}$	< 0.08	< 0.17			
< 0.3	< 0.2	$0.22^{+0.09}_{-0.11}$			
551.5 (582)	547.4 (572)	704.4 (745)			
	$0.7-11.8 \text{ keV}$ PL model 1.78 ± 0.03 6.8 ± 0.3 $562.5 (584)$ GAUSS model 1.81 ± 0.03 $6.4^{+0.4}_{-0.3}$ $6.5 (\text{fixed})$ $0.50 (\text{fixed})$ 0.20 ± 0.06 $551.7 (583)$ SS+PEXRAV r $1.83^{+0.06}_{-0.05}$ $6.1^{+0.6}_{-0.7}$ $6.50 (\text{fixed})$ $0.20^{+0.05}_{-0.06}$ < 0.3	$\begin{array}{cccccccccccccccccccccccccccccccccccc$			

Table 5: Results of fitting the measured XMM-Newton spectra by different models

of the order of several hours (here and below, all time intervals are given in the quasar rest frame) its X-ray luminosity exhibits no statistically significant variability. However, the luminosity changed noticeably from observation to observation in the fall of 2019, having increased approximately by 50% in ~ 25 days. A comparison of these new SRG and XMM-Newton measurements with the previous measurements of other X-ray observations showed that in the entire 17-year history of observations of the quasar PG 1634+706 its X-ray luminosity varied by no more than a factor of 2.5, while the variations on time scales of several weeks and several years are comparable in amplitude.

It is interesting to consider these results in the general context of X-ray AGN variability. Recently, based on a representative sample of X-ray bright quasars from SDSS, SRG/eROSITA all-sky survey data, and archival XMM-Newton data, Prokhorenko & Sazonov 2021 established that the characteristic X-ray variability amplitude for quasars increases slowly with time but decreases with luminosity. For quasars with a luminosity $\sim 10^{46}~\rm erg/s$ the characteristic variability amplitude (the ratio of a random pair of fluxes) on time scales of 10–20 years is ~ 1.4 with a significant dispersion from object to object. Thus, the quasar PG 1634+706 does not look remarkable as regards the X-ray variability among quasars with a comparable luminosity.

7 ACKNOWLEDGEMENTS

In this study we used data from the ART-XC and eROSITA telescopes onboard the SRG observatory. The SRG observatory was designed by the Lavochkin Association (enters into the Roskosmos State Corporation) with the participation of the Deutsches Zentrum fur Luft- und Raumfahrt (DLR) within the framework of the Russian Federal Space Program on the order of the Russian Academy of Sciences. The eROSITA X-ray telescope was built by a consortium of German Institutes led by MPE, and supported by DLR. The ART-XC team thanks the Roskosmos State Corporation, the Russian Academy of Sciences, and the Rosatom State Corporation for supporting the design and production of the ART-XC telescope and the Lavochkin Association and partners for the production and work with the spacecraft and the Navigator platform. The eROSITA data used in this work were processed with the eSASS software developed by the German eROSITA consortium and the proprietary data reduction and analysis software developed by the Russian eROSITA Consortium.

8 FUNDING

This study was supported by RSF grants nos. 21-12-00343 and 19-12-00396 with regard to the eROSITA and ART-XC data processing, respectively.

REFERENCES

```
Ananna T. T., et al., 2022, ApJS, 261, 9
Anders E., Grevesse N., 1989, Geochimica Cosmochimica Acta, 53, 197
Arnaud K. A., 1996, in Jacoby G. H., Barnes J., eds, Astronomical Society of the Pacific Conference Series Vol. 101, Astronomi-
```

cal Data Analysis Software and Systems V. p. 17 Boissay R., Ricci C., Paltani S., 2016, A&A, 588, A70

Brightman M., et al., 2013, MNRAS, 433, 2485

Elvis M. Lockman F. L. Wilkes B. L. 1080, AL 97, 777

Elvis M., Lockman F. J., Wilkes B. J., 1989, AJ, 97, 777

Elvis M., et al., 1994, ApJS, 95, 1

George I. M., Fabian A. C., 1991, MNRAS, 249, 352

George I. M., Turner T. J., Yaqoob T., Netzer H., Laor A., Mushotzky R. F., Nandra K., Takahashi T., 2000, ApJ, 531, 52

Green R. F., Schmidt M., Liebert J., 1986, ApJS, 61, 305 Guainazzi M., Bianchi S., 2007, MNRAS, 374, 1290

Haro-Corzo S. A. R., Binette L., Krongold Y., Benitez E., Humphrey A., Nicastro F., Rodríguez-Martínez M., 2007, ApJ, 662, 145

Jansen F., et al., 2001, A&A, 365, L1

Jiménez-Bailón E., Piconcelli E., Guainazzi M., Schartel N., Rodríguez-Pascual P. M., Santos-Lleó M., 2005, A&A, 435,

Jin C., Ward M., Done C., Gelbord J., 2012, MNRAS, 420, 1825
Kelly B. C., Bechtold J., Trump J. R., Vestergaard M., Siemiginowska A., 2008, ApJS, 176, 355

Khorunzhev G. A., Sazonov S. Y., Burenin R. A., Tkachenko A. Y., 2012, Astronomy Letters, 38, 475

Krawczyk C. M., Richards G. T., Mehta S. S., Vogeley M. S., Gallagher S. C., Leighly K. M., Ross N. P., Schneider D. P., 2013, ApJS, 206, 4

Lyke B. W., et al., 2020, ApJS, 250, 8

Magdziarz P., Zdziarski A. A., 1995, MNRAS, 273, 837

Malizia A., Sazonov S., Bassani L., Pian E., Beckmann V., Molina M., Mereminskiy I., Belanger G., 2020, New Astron. Rev., 90, 101545

Miller J. M., 2007, ARA&A, 45, 441

Nandra K., Fabian A. C., Brandt W. N., Kunieda H., Matsuoka M., Mihara T., Ogasaka Y., Terashima Y., 1995, MNRAS, 276, 1

Nayakshin S., Kazanas D., Kallman T. R., 2000, ApJ, 537, 833 Neeleman M., Prochaska J. X., Ribaudo J., Lehner N., Howk J. C., Rafelski M., Kanekar N., 2016, ApJ, 818, 113

Page K. L., Reeves J. N., O'Brien P. T., Turner M. J. L., Worrall D. M., 2004, MNRAS, 353, 133

Park T., van Dyk D. A., Siemiginowska A., 2008, ApJ, 688, 807 Pavlinsky M., et al., 2021, A&A, 650, A42

Piconcelli E., Jimenez-Bailón E., Guainazzi M., Schartel N., Rodríguez-Pascual P. M., Santos-Lleó M., 2005, A&A, 432, 15

Predehl P., et al., 2021, A&A, 647, A1

Prokhorenko S. A., Sazonov S. Y., 2021, Astronomy Letters, 47, 515

Ricci C., et al., 2017, ApJS, 233, 17

Richards G. T., et al., 2006, ApJS, 166, 470

Ross R. R., Fabian A. C., 2005, MNRAS, 358, 211

Sazonov S. Y., Ostriker J. P., Sunyaev R. A., 2004, MNRAS, 347,

Sazonov S., et al., 2012, ApJ, 757, 181

Shakura N. I., Sunyaev R. A., 1973, A&A, 24, 337

Shang Z., et al., 2011, ApJS, 196, 2

Shemmer O., Brandt W. N., Netzer H., Maiolino R., Kaspi S., 2008, ApJ, 682, 81

Shemmer O., et al., 2014, ApJ, 783, 116

Sunyaev R., et al., 2021, A&A, 656, A132

Tananbaum H., Avni Y., Green R. F., Schmidt M., Zamorani G., 1986, ApJ, 305, 57

Trakhtenbrot B., et al., 2017, MNRAS, 470, 800

Turner T. J., Pounds K. A., 1989, MNRAS, 240, 833

Turner T. J., George I. M., Nandra K., Turcan D., 1999, ApJ, 524, 667

Vasudevan R. V., Fabian A. C., 2007, MNRAS, 381, 1235

Vaughan S., Edelson R., Warwick R. S., Uttley P., 2003, MNRAS, 345, 1271

Wilms J., Allen A., McCray R., 2000, ApJ, 542, 914 de Rosa A., et al., 2012, MNRAS, 420, 2087

9 APPENDIX

Date	Observatory	OBSID	Exposure time, ks	References	$L_{\rm X},10^{45}~{\rm erg/s}$
1981-02-06	Einstein	5351	1.83	1, 4, 9	$7.0_{-1.4}^{+1.4}$
1991-03-15	ROSAT	700246	9.01	9	$6.76^{+0.04}_{-0.04}$
1994-05-02	ASCA	71036000	47.7	2, 3, 9	$11.1^{+0.4}_{-0.4}$
1999-08-21	Chandra	1269	10.83	7, 8, 9	$6.8^{+0.2}_{-0.2}$
2000-03-23	Chandra	47	5.39	8, 9	$10.2^{+0.4}_{-0.4}$
2000-03-23	Chandra	62	4.85	8, 9	$10.3_{-0.4}^{+0.4}$
2000-03-24	Chandra	69	4.86	8, 9	$10.1_{-0.4}^{+0.4}$
2000-03-24	Chandra	70	4.86	8, 9	$9.7^{+0.4}_{-0.4}$
2000-03-24	Chandra	71	4.41	8, 9	$10.3_{-0.5}^{+0.5}$
2002-11-22	XMM-Newton	143150101	13.7	4, 6, 5, 9	$12.5^{+0.4}_{-0.4}$
2007-06-29	Swift	36672001	1.32	9	$4.9_{-0.8}^{+1.0}$
2007-06-29	Swift	36673001	1.48	9	$5.9^{+1.0}_{-0.9}$
2007-07-11	Swift	36672002	7.34	9	$5.2^{+0.4}_{-0.4}$
2008-04-22	Swift	36671002	2.09	9	$8.8^{+1.0}_{-0.9}$
2008-04-24	Swift	36673002	2.56	9	$7.3^{+0.8}_{-0.7}$
2008-04-26	Swift	36671003	3	9	$8.8^{+0.8}_{-0.7}$
2008-05-15	Swift	90030001	3.72	9	$8.4^{+0.7}_{-0.7}$
2008-06-12	Swift	90030002	3.25	9	$5.5^{+0.7}_{-0.6}$
2009-01-18	Swift	90030003	2.75	9	$5.0_{-0.6}^{+0.7}$
2012-06-11	Swift	91438001	1.26	9	$6.8^{+1.2}_{-1.0}$
2012-06-18	Swift	91438002	0.37	9	9^{+3}_{-2}
2012-06-22	Swift	91438004	0.42	9	$8.4^{+2.5}_{-1.9}$
2012 - 06 - 25	Swift	91438005	0.17	9	9^{+4}_{-3}
2012-06-26	Swift	91438006	0.36	9	10^{+3}_{-2}
2012-06-28	Swift	91438007	0.5	9	$7.8^{+2.2}_{-1.7}$
2012-07-01	Swift	91438008	5.88	9	$11.5^{+0.7}_{-0.6}$
2019-09-29	SRG		48.3, 55.0	10	$6.31^{+0.11}_{-0.11}$
2019-10-20	SRG		37.7, 39.0	10	$7.13^{+0.05}_{-0.05}$
2019-10-25	XMM-Newton	852980501	14.4	10	$7.51_{-0.13}^{+0.13}$
2019-11-23	SRG		37.0, 38.3	10	$8.55^{+0.06}_{-0.06}$
2019-11-24	XMM-Newton	852980301	12.7	10	$9.43^{+0.15}_{-0.15}$
2019-11-26	XMM-Newton	852980401	17.3	10	$9.16^{+0.13}_{-0.13}$
2019-11-26	SRG		39.8	10	$8.40^{+0.07}_{-0.07}$

References: (1) Tananbaum et al. (1986), (2) Nandra et al. (1995), (3) George et al. (2000), (4) Page et al. (2004), (5) Jiménez-Bailón et al. (2005), (6) Piconcelli et al. (2005), (7) Haro-Corzo et al. (2007), (8) Park et al. (2008), (9) Shemmer et al. (2014), (10) this paper. $L_{\rm X}$ is the Galactic absorption-corrected luminosity in the 2–10 keV energy band in the quasar rest frame.

Table 6: History of X-ray observations of the quasar PG 1634+706